Ability of multiangle remote sensing observations to identify and distinguish mineral dust types: 2. Sensitivity over dark water

Olga V. Kalashnikova[1] and Ralph Kahn[1]

Received 10 October 2005; revised 3 February 2006; accepted 6 March 2006; published 7 June 2006.

[1] We explore the ability of multiangle, multispectral measurements, such as those from the Multiangle Imaging SpectroRadiometer (MISR), to retrieve mineral dust properties. We first investigate MISR sensitivity theoretically, to a selection of medium-mode particle shapes, to single-scattering albedo (SSA), and to the ratio of medium- to large-mode aerosol optical thickness (AOT). Favorable, but not ideal, viewing conditions over dark water are assumed, and new dust optical models are adopted. This study shows sensitivity to differences in the angular spectral signals of medium-mode shapes when column midvisible AOT is greater than ~0.15 for components contributing 15–20% or more to the AOT. MISR-like retrievals can also distinguish strongly absorbing (red channel SSA ~ 0.94) from less absorbing (SSA ~ 0.98–0.99) dust particles. Bimodal size sensitivity results suggest that MISR can distinguish the ratio of medium to larger components in roughly 20% midvisible AOT increments. For five Saharan dust field events over homogeneous, cloud-free dark water near the Cape Verde AERONET station, MISR research retrieval results were dominated by weakly absorbing medium grains. MISR-retrieved spectral AOT was within 0.02 of the Aerosol Robotic Network (AERONET), except for one spatially heterogeneous AOT > 1 case, and one where AERONET retrieved a significant component <0.1 μm in radius. In two cases where AERONET ran retrievals assuming nonspherical (spheroidal) particles, SSA fell within 0.02 of MISR. When included in the MISR Standard Aerosol Retrieval Algorithm, the new dust optical models improve both the coverage of successful retrievals and the spectral AOT agreement with near-coincident AERONET measurements. Large-mode dust models and available field constraint limitations are being addressed in continuing work.

Citation: Kalashnikova, O. V., and R. Kahn (2006), Ability of multiangle remote sensing observations to identify and distinguish mineral dust types: 2. Sensitivity over dark water, *J. Geophys. Res.*, *111*, D11207, doi:10.1029/2005JD006756.

1. Introduction

[2] Airborne mineral dust significantly affects atmospheric radiative properties on both local and global scales, during dust storms over the Asian and Saharan deserts, and as a consequence of long-range transport over oceans. Our understanding of the magnitude and even the sign of dust radiative forcing is highly uncertain compared to most other atmospheric aerosols, due to our incomplete knowledge of dust physical and optical properties, as well as the processes responsible for dust production, transport, and evolution [*Intergovernmental Panel on Climate Change*, 2001]. Together with field experiments, satellite observations of dust outbreaks, placed into the context of large-scale dust transport modeling, can reduce many of these uncertainties. Space-based multiangle imaging can play a special role in global aerosol studies because such data contain information about aerosol physical and optical properties [*Kahn et al.*, 1998, 2001a]. In particular, multiangle instruments are expected to distinguish the radiative signals of nonspherical and spherical particles, making it possible to separate mineral dust aerosols from other common aerosol components [*Kahn et al.*, 1997].

[3] The Multiangle Imaging SpectroRadiometer (MISR) instrument aboard the NASA Earth Observing System's Terra satellite was designed to view Earth in nine different directions, to detect angular variations of the sunlight reflected by aerosols, clouds and the planet's surface [*Diner et al.*, 1998, 2005]. Displaced symmetrically with respect to the nadir camera (designated An), the eight other cameras have nominal viewing angles of 70.5°, 60.0°, 45.6°, and 26.1° in the forward (Df, Cf, Bf, Af) and aft (Aa, Ba, Ca, Da) directions along the line of flight. Each camera images the underlying scene in four spectral bands centered at 446.4, 557.5, 671.7 and 866.4 nm with bandwidths of 41.9, 28.6, 21.9 and 39.7 nm, respectively. The time interval between the Df and Da camera observations of a 400 km

[1]Jet Propulsion Laboratory, California Institute of Technology, Pasadena, California, USA.

0148-0227/06/2005JD006756$09.00

cross-track line on the surface is about 7 min. MISR has high absolute radiometric accuracy of about 3% [*Bruegge et al.*, 2004]. The analysis presented here takes advantage of all these aspects of the MISR observations, for the red and near-infrared channels used in current aerosol retrievals over dark water (version 17 and below).

[4] This paper is the second in a series that explores MISR's dust-sensing abilities. *Kalashnikova et al.* [2005] (hereinafter referred to as paper 1) developed mineral dust optical models for composition-shape-size (CSS) distributions that were derived from recent field measurements of size and single-scattering albedo (SSA), combined with Individual Particle Analyses (IPA) of atmospheric dust sample size-dependent circularity and shape. Satellite aerosol retrieval algorithms require good particle optical models to account for the effects of shape and wavelength-dependent refractive index on particle single-scattering phase function, SSA, and spectral extinction properties [e.g., *Mishchenko et al.*, 1995]. Paper 1 produced dust optical analogs for medium-mode sphere, spheroid (aspect ratios equally distributed between 1.2 to 2.2), plate (2-D aspect ratio 1.5, height to width ratio 1/3, circularity distributed between 1.0 and 2.3), and grain (aspect ratio 1.5, height to width ratio 1, circularity distributed between 1.0 and 2.3) distributions, constrained by particle size and circularity field measurements. Spectral SSA was modeled using the Bruggeman effective medium approximation favored by *Sokolik and Toon* [1999], for internal mixtures of 1%, 2%, 4%, and 10% hematite, the most common absorbing species in most mineral dust samples.

[5] The Discrete Dipole Approximation (DDA) code [*Draine and Flatau*, 1994], used to model medium-mode particles, cannot simulate, for the MISR spectral bands, the optical properties of particles having volume-equivalent radii larger than about 0.7 μm, due to the excessive size of such computations. In paper 1, large-mode dust was modeled only with spheroids, using the less computationally demanding T-matrix approach [*Mishchenko et al.*, 2002]. This is a limitation of the dust optical analogs used here. It is mitigated in the current application because (1) MISR's longest wavelength is 867 nm, so the measurements are sensitive primarily to medium-mode particles ($PM_{2.5}$) [e.g., *Kahn et al.*, 1998, 2001a] and (2) for transported dust, the medium mode dominates. Paper 1 identified significant differences in the spectral angular optical properties relevant to MISR observations based on hematite content, and on medium-mode shape, and demonstrated good agreement between grain-shaped model phase functions and laboratory measurements. Other work in this field also demonstrates reasonable model/measurement agreement for particles modeled, for example, as Gausian random particles [*Volten et al.*, 2001] or as spheroids having very large eccentricities [*Kahnert et al.*, 2005]. More studies are needed to properly understand dust particle shapes for many remote sensing and climate applications.

[6] The current paper aims at assessing the dust aerosol property distinctions that can be made with MISR data. Section 2 presents a theoretical study that systematically explores MISR sensitivity to dust shape models used, SSA of dust types having 1, 2, 4 and 10% hematite, internally mixed, and medium- to large-particle ratio, under favorable but not ideal dark water viewing conditions. In section 3, we compare MISR operational and research retrieval results with near-coincident, Aerosol Robotic Network (AERONET)-derived spectral aerosol optical thickness (AOT), SSA, and size distribution near the Cape Verde island station, at times when Saharan dust dominates the atmospheric column. The paper concludes with a summary in section 4.

2. Theoretical Sensitivity Study

[7] We begin by systematically testing MISR sensitivity to a range of medium-mode shapes, SSA, and ratio of medium- to large-mode dust optical analogs. This must be done by theoretical simulation, since there are no well-characterized validation data sets rich enough to adequately cover the expected range of attributes; in section 3 we evaluate a series of available field cases for which ground truth exists. The aim of the sensitivity analysis is to quantify as much as possible the mineral dust shape, SSA, and size-mode ratio information content of MISR data, under cloud-free, dark water, low to modest wind speed conditions, with the understanding that as these conditions are relaxed, retrieval quality is likely to degrade.

[8] The analysis amounts to a refinement of previous theoretical sensitivity studies by *Kahn et al.* [1997, 1998, 2001a], making use of the new dust optical CSS models from paper 1. Prior work demonstrated MISR sensitivity to the difference between spherical and randomly oriented ellipsoidal Saharan dust analogs under good, dark water viewing conditions, for total column, midvisible AOT of about 0.15 or larger, and for aerosol components contributing at least about 20% to the column AOT [*Kahn et al.*, 1997].

[9] The current study adopts the MISR Research Aerosol Retrieval algorithm developed for previous sensitivity investigations. Unlike the MISR Standard Aerosol Retrieval algorithm, designed to automatically process the entire MISR global data stream with a fixed climatology of three-component aerosol mixtures [*Martonchik et al.*, 1998, 2002], the Research Retrieval analyzes measured or simulated pixel patches of any size, individually, and has the flexibility to test all combinations of up to four-component aerosol mixtures [*Kahn et al.*, 2001a].

2.1. Approach

[10] We investigate MISR sensitivity to mixtures of analog dust components having the following properties [*Kalashnikova et al.*, 2005]:

[11] 1. Components having a medium-mode particle shape are investigated: spheres, mixtures of randomly oriented oblate and prolate spheroids [*Mishchenko et al.*, 1997], mixtures of randomly oriented grains, and mixtures of randomly oriented plates, having uniform 2% hematite composition.

[12] 2. Medium-mode particle SSA for dust having 1, 2, 4, and 10% hematite content (by volume), internally mixed, are investigated.

[13] 3. Ratios of medium-mode and large-mode components are investigated. Medium-mode components are modeled as grains and spheroids having uniform 2% hematite composition. As in paper 1, the medium-mode, number-weighted lognormal size distribution has a fixed character-

Table 1. Physical and Optical Properties of Nonspherical Models Used in Theoretical MISR Sensitivity Studies[a]

Name	Shape	$r_{0\ N}$, μm	r_I, μm	r_{eff}, μm	σ	σ_{ext}, 0.672 μm	σ_{ext}, 0.866 μm	w_0, 0.672 μm	w_0, 0.866 μm
grains_1p_M1	grains	0.5	0.89	0.75	1.5	3.626	3.673	0.994	0.997
grains_2p_M1	grains	0.5	0.89	0.75	1.5	3.641	3.672	0.990	0.995
grains_4p_M1	grains	0.5	0.89	0.75	1.5	3.606	3.711	0.979	0.989
grains_10p_M1	grains	0.5	0.89	0.75	1.5	3.547	3.755	0.942	0.978
plates_1p_M1	plates	0.5	0.89	0.75	1.5	3.901	3.814	0.994	0.997
plates_2p_M1	plates	0.5	0.89	0.75	1.5	4.023	3.755	0.991	0.995
plates_4p_M1	plates	0.5	0.89	0.75	1.5	3.958	3.901	0.981	0.989
plates_10p_M1	plates	0.5	0.89	0.75	1.5	4.086	4.034	0.962	0.980
spheroidal_1p_M1	spheroids	0.5	0.89	0.75	1.5	3.533	3.847	0.991	0.995
spheroidal_2p_M1	spheroids	0.5	0.89	0.75	1.5	3.532	3.845	0.985	0.993
spheroidal_4p_M1	spheroids	0.5	0.89	0.75	1.5	3.461	3.800	0.968	0.985
spheroidal_10p_M1	spheroids	0.5	0.89	0.75	1.5	3.348	3.719	0.921	0.968
spheroidal_1p_M2	spheroids	1.0	2.94	2.40	2.0	2.307	2.380	0.970	0.983
spheroidal_2p_M2	spheroids	1.0	2.94	2.40	2.0	2.307	2.379	0.955	0.974
spheroidal_4p_M2	spheroids	1.0	2.94	2.40	2.0	2.303	2.375	0.905	0.946
spheroidal_10p_M2	spheroids	1.0	2.94	2.40	2.0	2.294	2.362	0.805	0.899
spheroidal_2p_M3	spheroids	1.5	3.36	2.93	2.0	2.224	2.354	0.955	0.974
spheroidal_2p_M4	spheroids	2.0	3.51	3.15	2.0	2.233	2.276	0.955	0.974

[a]Summarized from *Kalashnikova et al.* [2005]. Abbreviations are as follows: p, percent hematite, internally mixed; M, size mode (M1, medium; M2, large, $r_{0\ N}$ = 1 μm; M3, large, $r_{0\ N}$ = 1.5 μm; M4, large, $r_{0\ N}$ = 2 μm); $r_{0\ N}$, characteristic radius of number-weighted distribution; r_I, volume-weighted radius; r_{eff}, effective radius; σ, distribution standard deviation; σ_{ext}, extinction coefficient; w_0, single-scattering albedo. See text for details about the size distributions used.

istic radius of 0.5 μm and σ of 1.5. The large-mode particles, concentrated near dust sources, vary in size more than medium mode particles [*Clarke et al.*, 2004], and are modeled in three sizes given in point 3 above. Large-mode components are modeled as spheroids having1, 2, 4, and 10% hematite, number-weighted lognormal size distributions of r_0 = 1 μm (M2), 1.5 μm (M3) and 2 μm (M4), and standard deviation (σ) of 2.0.

[14] Wavelength-dependent SSA, extinction efficiency, and scattering phase function for these components were derived in paper 1. Table 1 summarizes the shapes, sizes, spectral extinction efficiencies, and SSA of these particles. Particle scattering phase functions for the 2% hematite components are plotted in Figure 1 for the MISR green (0.552 μm) channel and the selected dust shapes and size modes, along with that of the 20 μm, randomly oriented hexagonal prism cirrus optical analog from *Takano and Liou* [1989].

[15] The MISR Research Aerosol Retrieval algorithm allows us to compare modeled (or measured) MISR top of atmosphere (TOA) reflectances for a reference "atmosphere" with modeled "comparison" reflectances for mixtures of up to four components, in all proportions at 5% increments [*Kahn et al.*, 2001a]. For a dark water surface, the algorithm assumes Fresnel reflection, plus a standard wind speed–dependent whitecap model, as is also used in the MISR Operational Aerosol Retrieval algorithm [*Kahn et al.*, 2001b; *Martonchik et al.*, 1998]. As in previous studies,

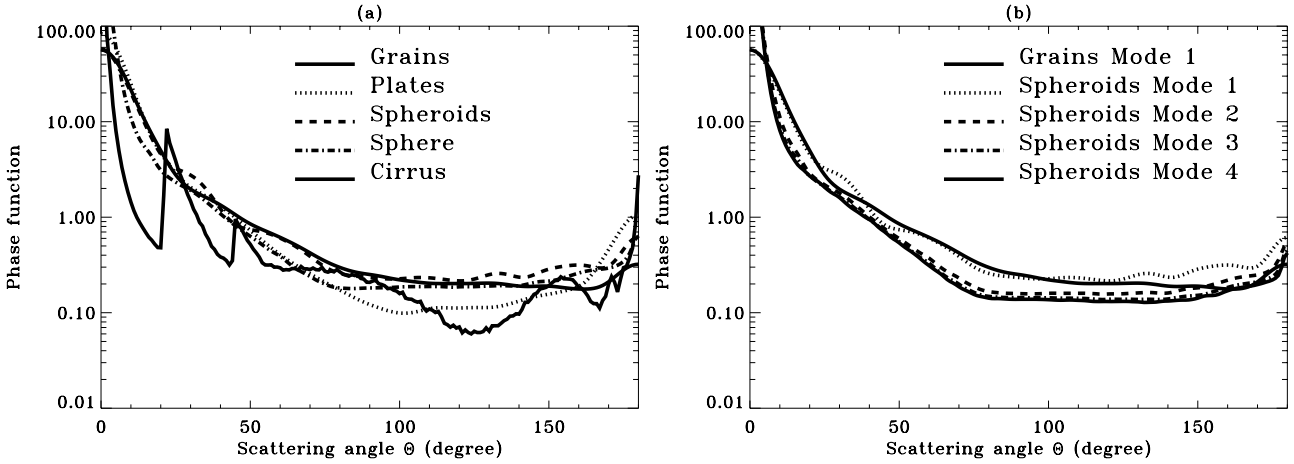

Figure 1. MISR 0.550 μm channel single-scattering phase functions for dust analog components having 2% hematite (a) for different shapes and (b) for different size mode spheroids plus a grain model. A cirrus model from *Takano and Liou* [1989] is also shown. "Mode" indicates the size mode of a number-weighted size distribution (1, medium, r_0 = 0.5 μm; 2, large, r_0 = 1 μm; 3, large, r_0 = 1.5 μm; 4, large, r_0 = 2 μm). Adapted from *Kalashnikova et al.* [2005].

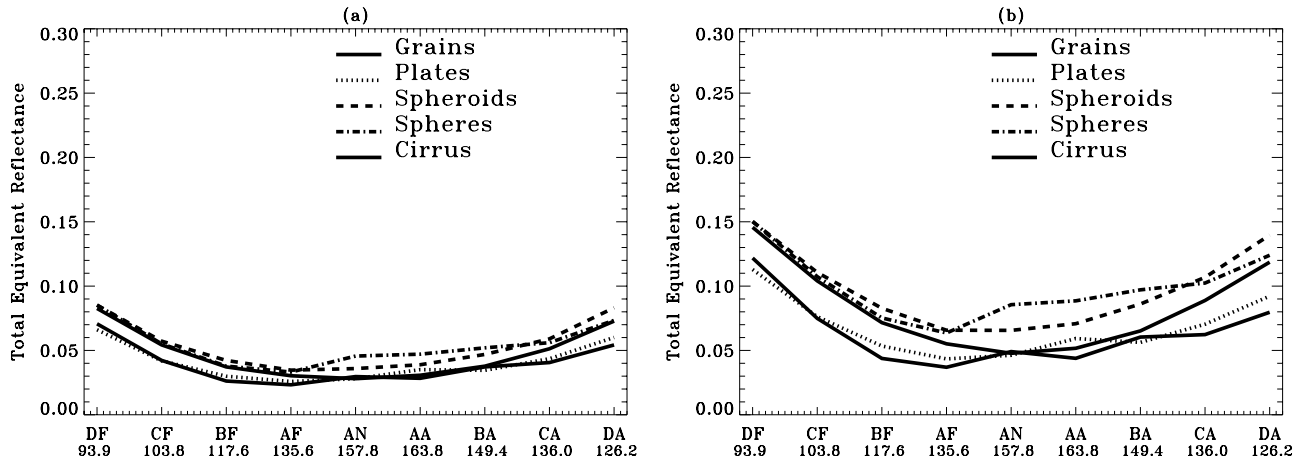

Figure 2. Top of atmosphere (TOA) reflectances versus MISR view angle, calculated for atmospheres containing individual medium-mode, 2% hematite components and illustrating the impact of shape on the observed red band (0.672 μm) MISR signal for total column midvisible optical depths (a) 0.2 and (b) 0.5.

we adopt midlatitude geometry, and mix all aerosol components in the lower atmosphere with a scale height of 2 km; alternative, reasonable vertical distributions have a negligible effect on retrieval results unless the component aerosols are very absorbing.

[16] Comparison model TOA reflectances are tested against reference atmosphere reflectances based on the χ^2_{max} threshold value [*Kahn et al.*, 1998, 2001a]. For each comparison, χ^2_{max} is the maximum of three separate tests variables, χ^2_{geom}, χ^2_{spec}, and χ^2_{abs}, that account for camera to camera, band to band, and absolute reflectance differences, respectively, between the comparison model and reference atmosphere.

[17] Individual cases amount to different choices of reference atmosphere components, against which comparison models are tested, and all models that meet the acceptance criterion are included in the solution space. For each case examined, we consider reference atmospheres having column green band AOT of 0.2, 0.5 and 1.0, take near-surface wind speeds of 0, 2.5, and 5 m/s, and set χ^2_{max} thresholds for acceptable matches to 1 and 2. Further discussion of the Research Aerosol Retrieval algorithm and sensitivity study approach is given in the references cited above.

2.2. Sensitivity to Medium-Mode Particle Shape

[18] Figure 2 illustrates the impact particle shape can have on MISR signals. Calculated red band TOA reflectances for atmospheres containing individual, medium-mode components having different shapes, are plotted against MISR view angle for several column AOT values. Grains, plates, spheroids, spheres, and cirrus each produce distinct angular signatures in this example. Broadly, plates and cirrus show a pattern in the forward versus aft-viewing cameras that differs from the other shapes, even at 0.2 midvisible AOT. The sphere, spheroid, and grain signatures are distinct in the aft views, where the scattering angle exceeds 120°. The TOA reflectance differences for these shapes increase with AOT, as expected.

[19] To test MISR sensitivity to medium-mode particle shape, we address the question: If the atmosphere contains particles of a certain shape, with fixed SSA and medium-mode size, could MISR retrievals interpret the measured reflectances as due to particles having a different shape with the same SSA and size mode? The SSA and size dimensions are explored in subsequent sections. Here we choose particles internally mixed with 2% hematite for reasons covered in section 2.3 below. For the cases shown, the atmosphere, the near-surface wind speed is set to 2.5 m/s (though the comparison models cover 0, 2.5, and 5 m/s).

[20] Figure 3a reports the key medium-mode shape sensitivity analysis results when the atmosphere contains grains. Tests were performed for reference atmosphere AOT values of 0.2, 0.5, and 1.0 (the 1.0 cases are not shown since they are nearly identical to those for 0.5), and for comparison models composed of four-component mixtures containing all possible proportions, in 5% increments, of medium-mode grains, plates, spheres, spheroids. Comparison models containing cirrus were mixed in all proportions with medium-mode plates, grains, and spheres. Even when the χ^2_{max} threshold is set to 2 and the atmosphere AOT is 0.2, the loosest combination of criteria we applied (Figure 3a, left), all acceptable comparison mixtures contain at least 80% grains. As expected, the solution space narrows

Figure 3. Medium-mode shape sensitivity plots. Four pairs of bar charts are shown. The simulated atmosphere for each pair contains an individual medium-mode (r_0 = 0.5 μm) component of (a) grains, (b) plates, (c) spheroids, and (d) spheres, all having 2% hematite internally mixed. For each pair the left plot has midvisible AOT = 0.2 for the atmosphere, and the comparison model acceptance criterion is $\chi_{max}{}^2 < 2$. For the right plot, AOT = 0.5, and $\chi_{max}{}^2 < 1$. The black bars indicate, for each shape component in the analysis, the range of percent midvisible AOT for which the criterion was met. A nominal wind speed of 2.5 m/s is assumed for the cases shown. The four-dimensional comparison model space is described in the text.

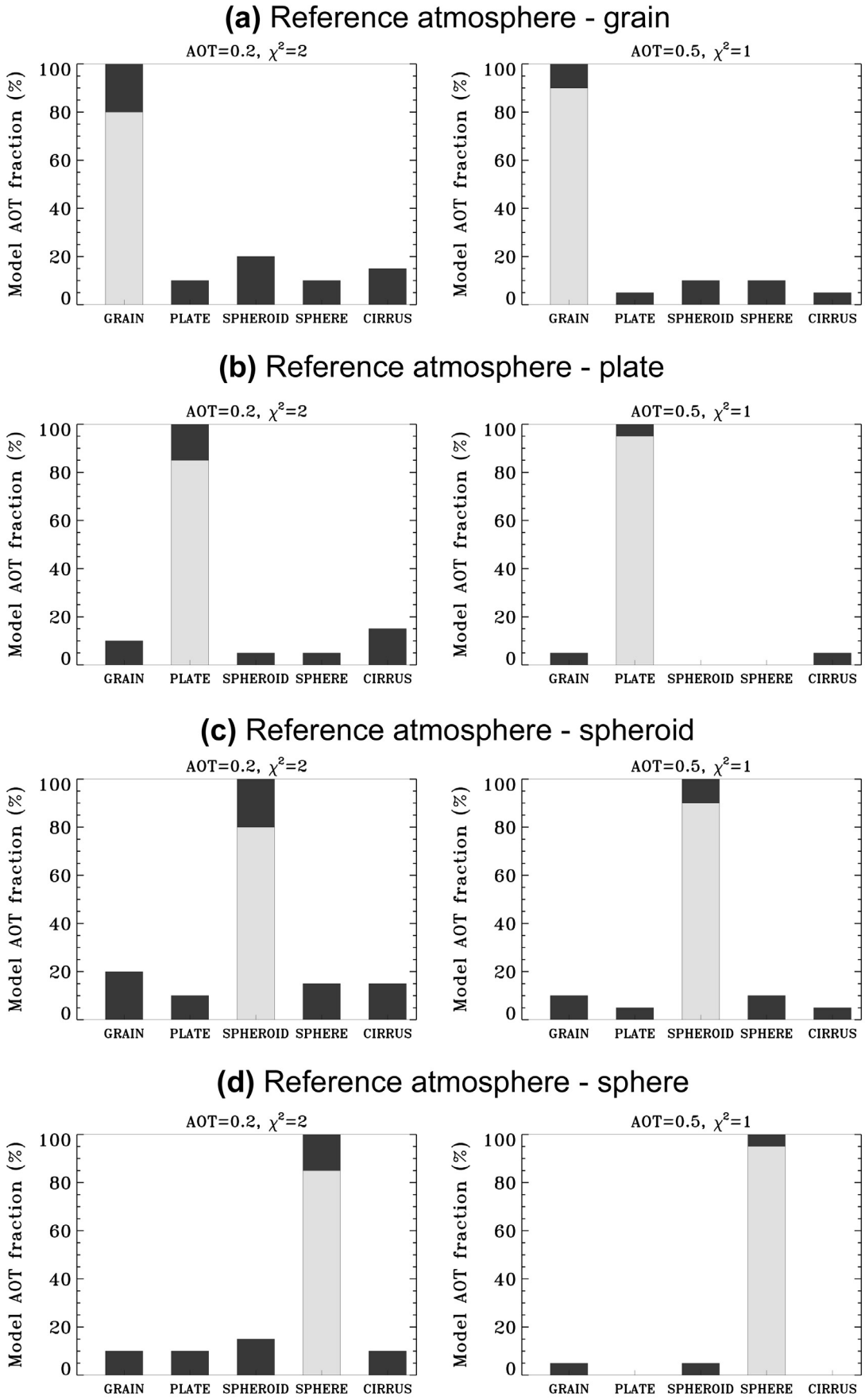
(a) Reference atmosphere - grain
AOT=0.2, χ^2=2
AOT=0.5, χ^2=1
(b) Reference atmosphere - plate
AOT=0.2, χ^2=2
AOT=0.5, χ^2=1
(c) Reference atmosphere - spheroid
AOT=0.2, χ^2=2
AOT=0.5, χ^2=1
(d) Reference atmosphere - sphere
AOT=0.2, χ^2=2
AOT=0.5, χ^2=1
Model AOT fraction (%)
0
20
40
60
80
100
GRAIN
PLATE
SPHEROID
SPHERE
CIRRUS

Figure 3

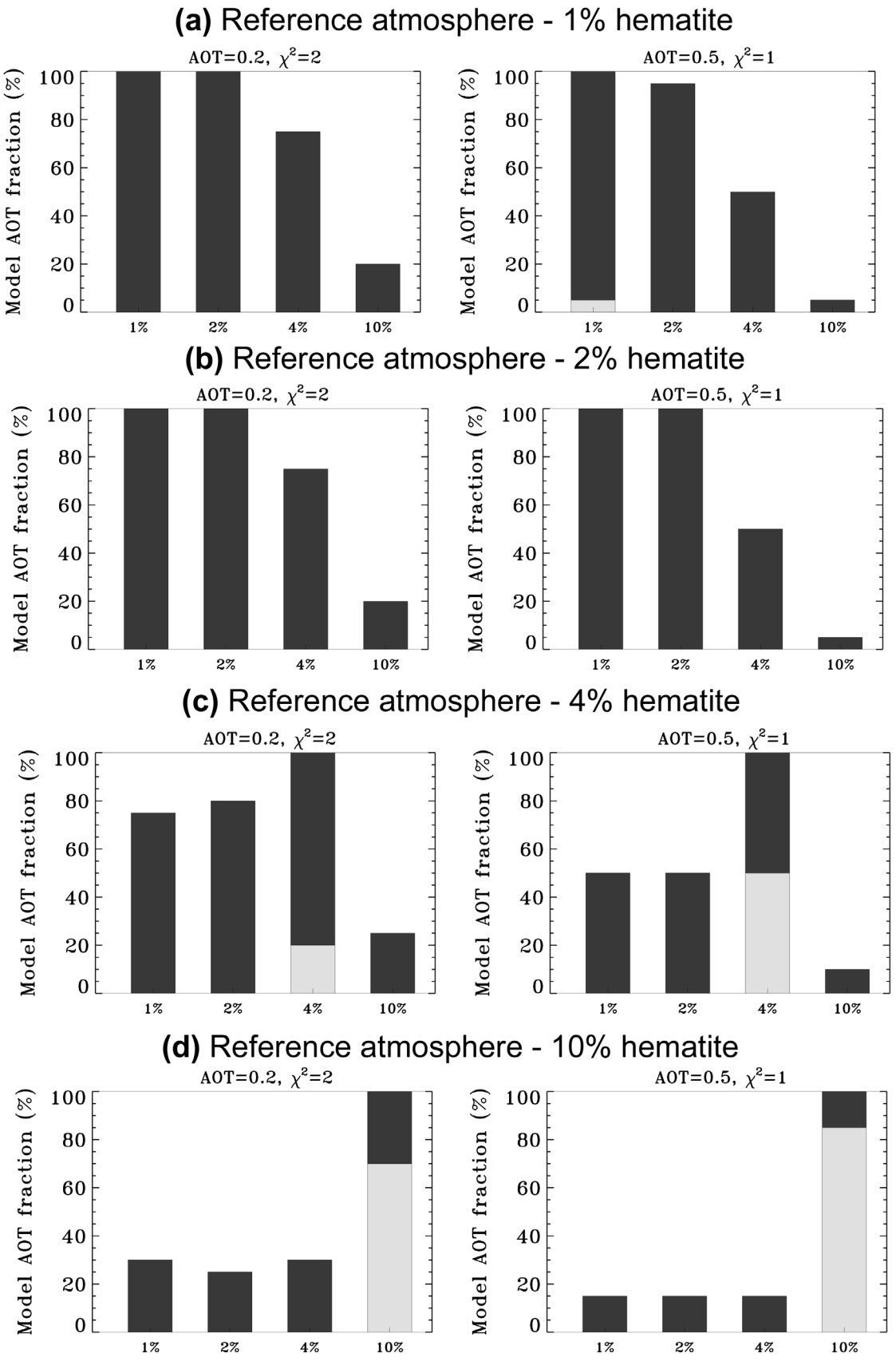
(a) Reference atmosphere - 1% hematite
AOT=0.2, χ^2=2
AOT=0.5, χ^2=1
(b) Reference atmosphere - 2% hematite
AOT=0.2, χ^2=2
AOT=0.5, χ^2=1
(c) Reference atmosphere - 4% hematite
AOT=0.2, χ^2=2
AOT=0.5, χ^2=1
(d) Reference atmosphere - 10% hematite
AOT=0.2, χ^2=2
AOT=0.5, χ^2=1
Model AOT fraction (%)
0
20
40
60
80
100
1%
2%
4%
10%

Figure 4

further as the reference atmosphere AOT increases and as the χ^2_{max} threshold is reduced. These results are unaffected when the wind speed is decreased to zero, and sensitivity is reduced by no more than 5% when it is increased to 5 m/s. In all cases, shape discrimination diminishes when reference atmosphere AOT is reduced below about 0.15, manifesting an overall lack of information about particle properties when the atmosphere contains few aerosols.

[21] The remaining plot pairs in Figure 3 provide the corresponding results for reference atmospheres containing plates, spheroids, and spheres. Again the algorithm selects at least 80% of the correct atmospheric component shape, and when the χ^2_{max} threshold is set to 1, that limit is 90%. These MISR shape sensitivity results produce similar uncertainty ranges to those for size and sphericity in previous studies [*Kahn et al.*, 2001a], but provide considerably more detail about particle shape discrimination.

[22] Sensitivity tests for cirrus atmospheres versus plates and grains produce a maximum uncertainty of 15% for a χ^2_{max} threshold of 2, and 10% when it is reduced to 1. The MISR Standard Retrieval preference for cirrus models over some thick dust plumes [*Kalashnikova et al.*, 2005] might suggest an association of thin cirrus with dust outbreaks. The MISR Standard Aerosol retrieval algorithm climatology (for versions 16 and 17 of the product) contains mineral dust analogs from paper 1, but no cirrus analogs. It is likely that when cirrus is so thin that it is not detected by the cloud masks, the aerosol algorithm finds a best fit, among the available choices, with the large, nonspherical, weakly absorbing dust analogs. This issue is being investigated further in separate studies, with cases having near-coincident data from other instruments such as lidar.

2.3. Sensitivity to Medium-Mode Particle Single-Scattering Albedo

[23] Previous sensitivity studies indicate that at least for spherical particles, over the typical range of aerosol SSA values, we would not expect to distinguish more than two to four groupings in the MISR data based on SSA, under good but not ideal viewing conditions [*Kahn et al.*, 1998]. For mineral dust, we model SSA using internally mixed hematite, as discussed in paper 1. Here we begin by addressing the question: If the atmosphere contains medium-mode grains containing 1%, 2%, 4%, or 10% hematite, what ranges of particle SSA produce simulated TOA reflectances that acceptably match those of the modeled atmosphere? We also ask this question relating to plates, spheroids, and spheres.

[24] The results for grains, with near-surface wind speed for the reference atmosphere (but not for the comparison models) set to 2.5 m/s, are shown in Figure 4. The upper left pair (Figure 4a) reports sensitivity performance for reference atmosphere particles containing 1% hematite. Following the approach used for the shape study, reference atmosphere AOT values were set to 0.2, 0.5, and 1.0 (1.0 not shown because they are nearly identical to the 0.5 cases), χ^2_{max} thresholds of 2 for AOT = 0.2 (the least constrained conditions of this test) and 1 for AOT = 0.5 (the most constrained conditions) are included, and comparison models composed of four-component mixtures containing all possible proportions of 1%, 2%, 4%, and 10% hematite, in 5% increments, were tested. The other three blocks in Figure 4 provide corresponding plots for reference atmosphere particles containing 2% (Figure 4b), 4% (Figure 4c), and 10% (Figure 4d) hematite.

[25] For the 1% and 2% weakly absorbing atmospheres, the solution space includes comparison models containing as much as 100% of the correct atmospheric component. But acceptable matches are also found for mixtures containing up to 100% of the other weakly absorbing component, even when the χ^2_{max} threshold is set to 1 and the atmosphere AOT is 0.5 However, MISR can achieve about 50% sensitivity to the difference between the 1–2% models and the 4% model for the better-constrained situations, and 20% or better sensitivity to the difference between the weakly absorbing particles containing 1, 2, or 4% hematite, and those containing 10% hematite, even for the poorly constrained cases. Again, sensitivities are similar for no-wind conditions and uncertainties increase by no more than 5% for wind speeds of 5 m/s. The corresponding sensitivity analyses for the other shapes (not shown) produce essentially the same conclusions.

[26] These results indicate that over dark water, we can expect MISR to distinguish between weakly absorbing (4% or less hematite) and strongly absorbing (10% hematite) dust components. But from these results, the data over the dark water do not contain the information needed to distinguish among components having 4% hematite or less, which represents a range of MISR red and near-infrared band SSA between about 0.94 and 1.0 (Table 1). MISR sensitivity may improve for optically thick dust plumes, when all four MISR spectral bands are used, since the largest dust absorption differences occur in the blue and green bands [e.g., *Sokolik and Toon*, 1999]. However, in the shorter-wavelength bands, other factors such as dust layer height can become significant factors in retrieval accuracy [e.g., *Kahn et al.*, 2001a, 2001b]. Since recent field measurement analyses reviewed in paper 1 find that both Saharan and Asian mineral dust contain less than 4% hematite, we modeled SSA for the shape and size sensitivity analyses in sections 2.2 and 2.4 with 2% internally mixed hematite components.

2.4. Sensitivity to the Ratio of Medium-Mode to Large-Mode Components

[27] We now explore MISR sensitivity to the proportions of medium and large-mode components in aerosol mixtures, using the number-weighted lognormal size distributions

Figure 4. Four pairs of SSA sensitivity plots, arranged similarly to Figure 3. The simulated atmosphere for each pair contains an individual medium-mode (r_0 = 0.5 μm) grain-shaped component with (a) 1%, (b) 2%, (c) 4%, and (d) 10% internally mixed hematite. For each pair the left plot has midvisible AOT = 0.2 for the atmosphere, and the comparison model acceptance criterion is $\chi^2_{max} < 2$. For the right plot, AOT = 0.5, and $\chi^2_{max} < 1$. The black bars indicate, for each SSA component in the four-dimensional comparison space, the range of percent midvisible AOT for which the criterion was met. A nominal wind speed of 2.5 m/s is assumed for the cases shown.

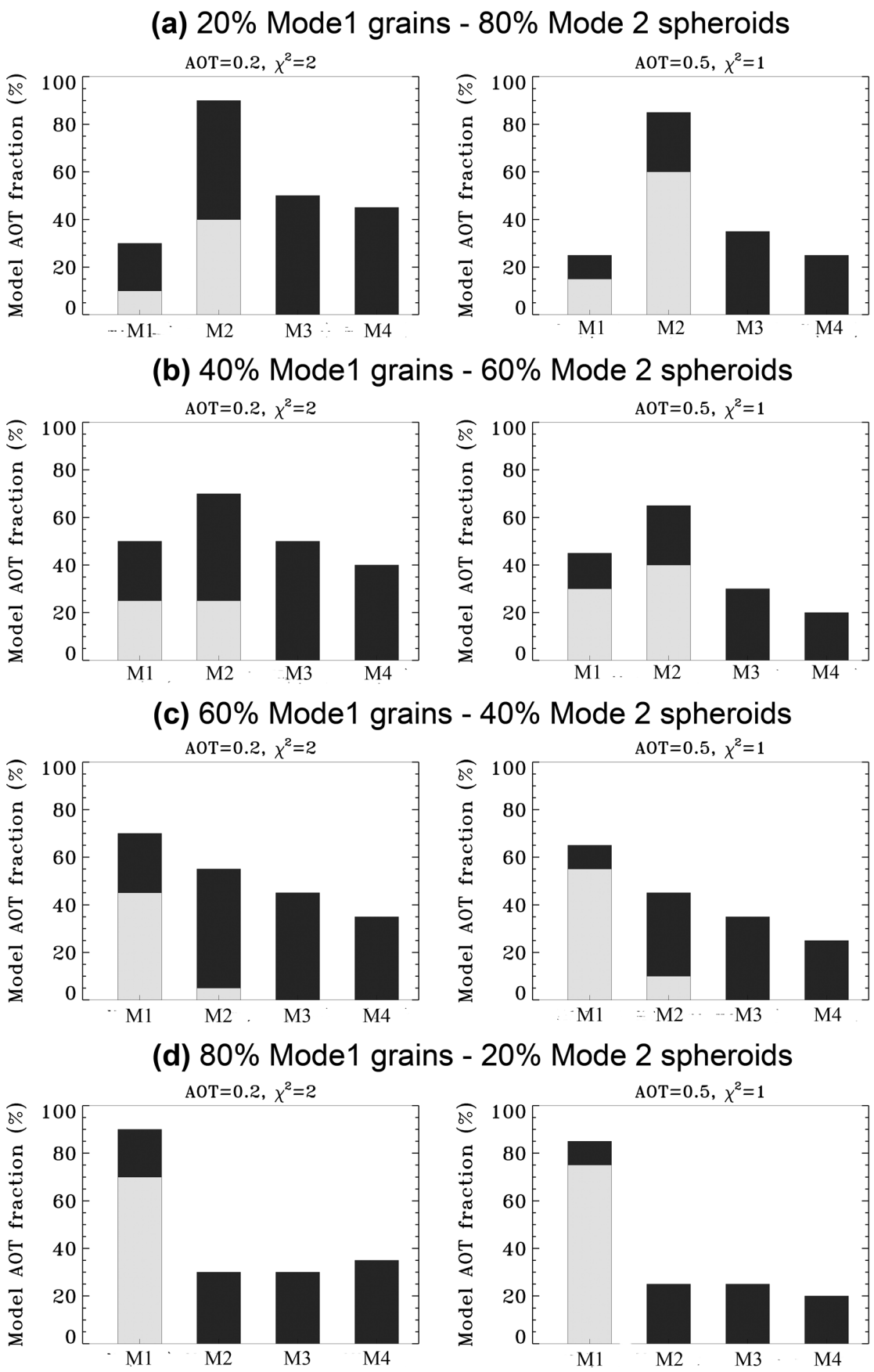
(a) 20% Mode1 grains - 80% Mode 2 spheroids
AOT=0.2, χ^2=2
AOT=0.5, χ^2=1
(b) 40% Mode1 grains - 60% Mode 2 spheroids
AOT=0.2, χ^2=2
AOT=0.5, χ^2=1
(c) 60% Mode1 grains - 40% Mode 2 spheroids
AOT=0.2, χ^2=2
AOT=0.5, χ^2=1
(d) 80% Mode1 grains - 20% Mode 2 spheroids
AOT=0.2, χ^2=2
AOT=0.5, χ^2=1
Model AOT fraction (%)
0
20
40
60
80
100
M1
M2
M3
M4

Figure 5

described in section 2.1. Included are medium-mode (M1, 0.5 μm characteristic radius) grains and spheroids, and large-mode, 1 μm (M2)., 1.5 μm (M3), and 2 μm (M4) characteristic radius spheroids, all having 2% hematite internally mixed, as discussed in section 2.3. Using 20% of the midvisible AOT as a rough value for the uncertainty in MISR-retrieved individual components, we select for this analysis bimodal reference atmospheres having 80, 60, 40 and 20% of a medium-mode component, mixed, correspondingly, with 20, 40, 60 and 80% of a large-mode component. As before, the comparison space includes mixtures of four components, in all possible proportions at 5% increments.

[28] Figure 5 is arranged similarly to the previous sensitivity study figures, showing results for reference atmospheres containing bimodal mixtures of the medium-mode M1 grain-shaped component and the large-mode M2 spheroid-shaped component, in midvisible AOT proportions of 20%–80% (Figure 5a), 40%–60% (Figure 5b), 60%–40% (Figure 5c), and 80%–20% (Figure 5d). All components in this figure contain 2% hematite, internally mixed. The comparison space includes these two components, plus M3 and M4 size spheroids having 2% hematite internally mixed. Figure 6 show results for the same reference atmospheres and for a comparison space that includes the 2% hematite M1 medium-mode grain-shaped component and the 2% hematite M2 large-mode spheroid-shaped component, plus M2 spheroids having 4% and 10% hematite.

[29] Figures 5 and 6 (and related tests not shown) demonstrate that MISR retrieval sensitivities to the properties of the large-size mode increase with increasing mode 2 loading, for total column AOT in the range 0.2 to 1.0. For 20% of mode 2, MISR retrievals are not sensitive to mode 2 properties; they select 70 to 90% of mode 1 along with any other large-sized models in the comparison space, for χ^2_{max} test thresholds of either 1 or 2. But for mode 2 loading above 20%, MISR becomes sensitive to some mode 2 proprieties. For 40% mode 2 loading, MISR retrievals are able to distinguish mode 1 from mode 2 AOT, and to separate mode 2 particles having 2 and 10% hematite, but they cannot distinguish among the M2, M3 and M4 spheroidal models. For 60% mode 2 loading, the MISR Research Retrieval is able to distinguish large-sized particles having 2 and 10% hematite, and those having M2 and M4 sizes.

[30] Figure 7 extends the results of Figures 5 and 6, showing what happens when the reference atmosphere and comparison space contain medium-mode ellipsoids rather than grains. Here we show only the 80%–20% and the 20%–80% results, when the comparison space contains different sized large-mode particles (Figures 7a and 7c) and different SSA large-mode particles (Figures 7b and 7d). The conclusions for spheroids are similar to those that include medium-mode grains.

[31] The bimodal sensitivity results suggest that under good viewing conditions, MISR can distinguish the ratio of medium to larger components in roughly 20% midvisible AOT increments, and can also retrieve some properties of a component in the bimodal mixture, provided the mixture contains more than 20% of that component. A similar conclusion was reached for a broader but less detailed selection of particle types by *Kahn et al.* [2001a].

[32] In the next section, we look at retrievals from actual MISR observations rather than theory, and compare the results with expectations based on the conclusions of the theoretical sensitivity study presented in this section.

3. Case Studies: MISR Retrievals for Dust Events Over Cape Verde

[33] Currently, coordinated aircraft, spacecraft, and surface observations are required to fully validate under natural conditions the column-averaged size, shape, and SSA constraints that the sensitivity analysis in section 2 suggests should be possible with MISR data. Such observations may be acquired during intensive field campaigns [e.g., *Kahn et al.*, 2004], but despite our efforts during the PRIDE, ACE-Asia, and UAE-2 campaigns, we have not yet obtained a well-constrained set of field data, near-coincident with a MISR overpass under dusty conditions, uncontaminated by significant clouds or pollution. To test as much as possible the MISR results, we rely here instead on dust microphysical property measurements taken at other times during PRIDE and ACE-Asia to characterize typical Saharan and Asian dust, respectively, as covered in paper 1, and use near-coincident AERONET spectral optical depth [*Holben et al.*, 1998], size, and SSA retrievals [*Dubovik and King*, 2000; *Dubovik et al.*, 2002a, 2002b] in situations where dust dominates the atmospheric aerosol.

[34] Five such dust events, observed by MISR and the Cape Verde Islands AERONET station, are analyzed in this section. These events were selected to represent the following situations (see Table 2 and Figure 8): (1) AERONET-retrieved AOTs in the range 0.3–0.4 (26 May and 11 June 2003); (2) AERONET-retrieved AOTs in the range 0.5–0.6 (6 and 8 February 2004); and (3) AERONET-retrieved AOT larger than 1 (6 June 2004).

[35] For each event, we selected two 3.3 × 3.3 km, uniform, dark water patches near the AERONET site for

Figure 5. Size-mode ratio sensitivity plots for medium-mode grains, with a comparison space that contains a range of large-mode size options along with the medium-mode particles. The plots are arranged in four pairs of bar charts, similarly to Figure 3. The simulated atmosphere for each pair contains a medium-mode (r_0 = 0.5 μm) grain-shaped component and a large-mode (M2, r_0 = 1 μm) spheroid-shaped component, mixed in midvisible AOT proportions of (a) 20%–80%, (b) 40%–60%, (c) 60%–40%, and (d) 80%–20%, all components having 2% internally mixed hematite. The comparison space includes these components plus M3 (r_0 = 1.5 μm) and M4 (r_0 = 2 μm) large-mode, spheroid-shaped components. For each pair the left plot has midvisible AOT = 0.2 for the atmosphere, and the comparison model acceptance criterion is $\chi^2_{max} < 2$. For the right plot, AOT = 0.5, and $\chi^2_{max} < 1$. The black bars indicate, for each component in the four-dimensional comparison space, the range of percent midvisible AOT for which the criterion was met. A nominal wind speed of 2.5 m/s is assumed for the cases shown.

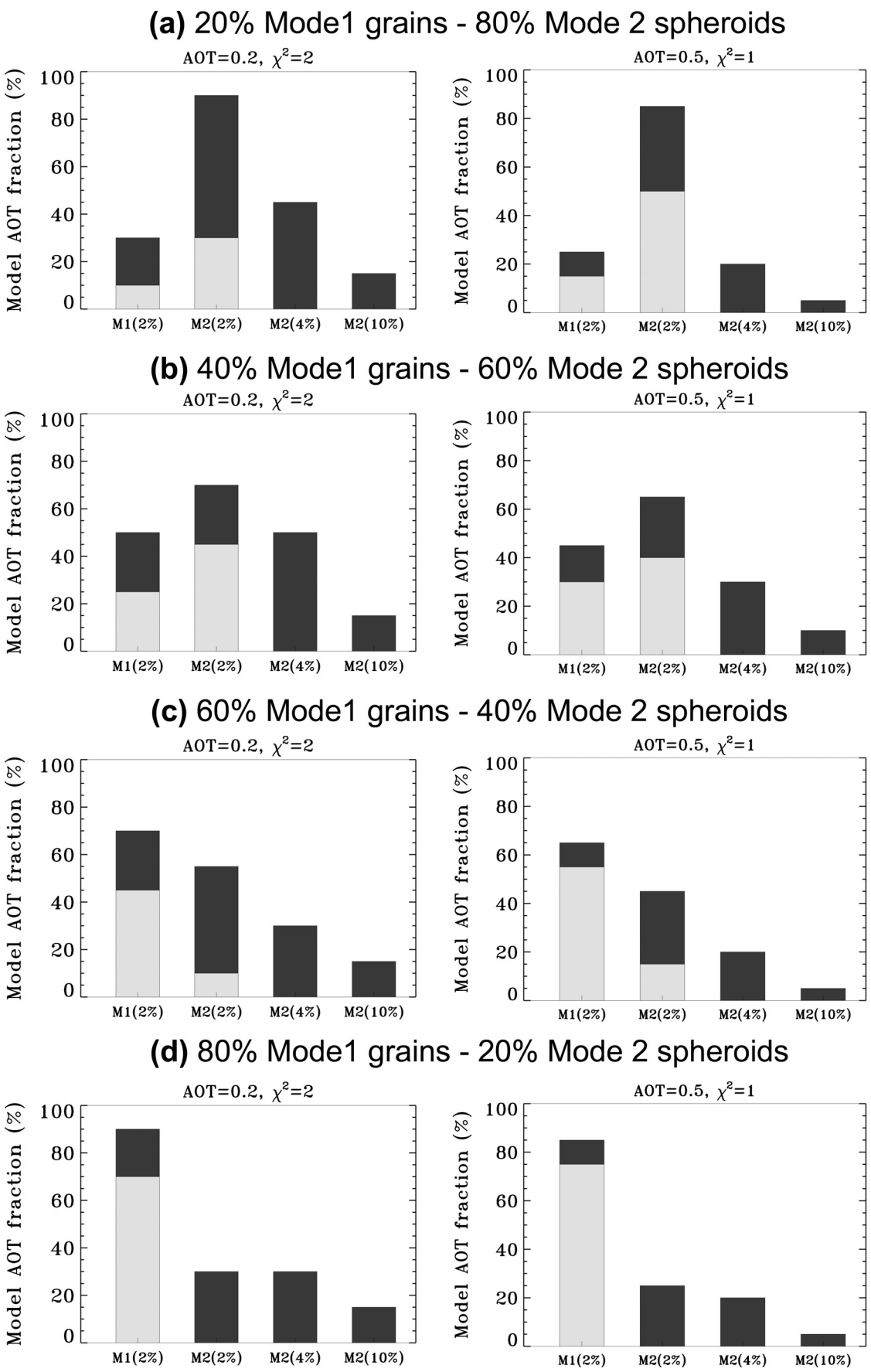
(a) 20% Mode1 grains - 80% Mode 2 spheroids
AOT=0.2, χ^2=2
AOT=0.5, χ^2=1
(b) 40% Mode1 grains - 60% Mode 2 spheroids
AOT=0.2, χ^2=2
AOT=0.5, χ^2=1
(c) 60% Mode1 grains - 40% Mode 2 spheroids
AOT=0.2, χ^2=2
AOT=0.5, χ^2=1
(d) 80% Mode1 grains - 20% Mode 2 spheroids
AOT=0.2, χ^2=2
AOT=0.5, χ^2=1
Model AOT fraction (%)
0
20
40
60
80
100
M1(2%)
M2(2%)
M2(4%)
M2(10%)

Figure 6

detailed analysis. Patch locations and AERONET-retrieved size distributions are shown in Figure 8. AERONET size distributions are routinely presented as volume-weighted quantities. So in this section, we report both number-weighted effective radius (r_{eff}), as we did in section 2, and volume-weighted radius r_V. Note that the volume-weighted quantities give greater weight to the larger particles than do the number-weighted ones. Latitudes and longitudes of MISR and AERONET sampling sites, together with the MISR overpass and AERONET sky-scan data collection times, are summarized in Table 2 for the five dust events in our study.

[36] In our analysis we use two types of AERONET measurements: direct Sun, that are routinely made every 15 min when possible, and sky-scan, that are made about once per hour under good conditions. The AERONET spectral AOTs come from the direct Sun observations, whereas AERONET size distributions and SSAs come from sky-scan retrievals [*Dubovik and King*, 2000]. We averaged with equal weight all AERONET direct Sun measurements within ±1 hour of the MISR overpass time for the MISR-AERONET spectral AOT comparisons. However, in a 2 hour window, only one sky-scan data point was available for each event.

[37] To analyze in detail MISR data information content about aerosol optical properties such as SSA and Angstrom exponent, we use the capabilities of the MISR Research Aerosol Retrieval used for the sensitivity study and described in section 2.1. The assumed aerosol climatology for these retrievals includes the dust particles listed in Table 1, as well as other common maritime aerosol component analogs given in Table 3.

[38] The best-fitting models selected by the Research Retrieval algorithm are summarized in Table 4. They all meet the condition $\chi^2_{\text{max}} < \sim 2$, and show that the number-weighted size parameters of best-fitting MISR Research Retrieval aerosol mixtures are generally in good agreement with the corresponding AERONET-retrieved values. On 6 February and 6 June 2004, when AERONET retrieves primarily medium-sized particles, the MISR Research Retrieval selected between 70% and 100% medium-sized, grain-shaped dust. MISR-retrieved r_{eff} and r_V agree with AERONET-retrieved values to within the uncertainty range predicted by the dust sensitivity study of section 2 above. The r_v are farther apart, since even the "narrow" AERONET size distributions include more large particles than the MISR ones, r_v emphasizes this spread in values, and MISR has limited sensitivity to microphysical properties of the larger particles.

[39] On 26 May and 11 June 2003 when AERONET retrieves a wider size distribution, MISR parallels this result, also selecting up to 30% AOT fraction of large-size particles. Again the MISR r_{eff} are somewhat larger than the corresponding AERONET values, and the reverse is true for r_v. In part, MISR sensitivity to microphysical properties is expected to decrease for particles larger than 1 μm radius (2 μm diameter), since the longest wavelength observed by MISR is 0.866 μm, and MISR is primarily sensitive to $PM_{2.5}$ [*Kahn et al.*, 1998]. In addition, the large-sized dust models currently available in the MISR retrievals are ellipsoids, and may need improvement to give a more acceptable fit to observed radiances [*Kalashnikova et al.*, 2005]. It also should be noted that the expected accuracy of AERONET size distribution and SSA retrievals decreases when AOT < 0.4 (e.g., the 26 May and 11 June cases), and AERONET expected accuracy is only 15–25% for radii larger than 0.5. These results indicate the relative uncertainty of MISR and AERONET aerosol-size retrievals; neither retrieved size distribution has as yet been validated with independent field data in these dusty situations. From the results available here, we conclude that generally, MISR can retrieve three to five size bins over the $PM_{2.5}$ size range, as expected from sensitivity studies (see section 2 above and *Kahn et al.* [1997, 1998]).

[40] On 8 February, MISR retrieved larger total r_{eff} and r_V than AERONET. The discrepancy is due in part to the strongly bimodal AERONET-retrieved size distribution, since MISR has limited sensitivity to particles smaller than about 0.1 μm radius. The AERONET-retrieved coarse mode r_V on this day is 1.45, larger than the MISR-retrieved value of 0.92. However, it should be noted that AERONET retrievals consider all particles smaller than 0.6 μm as fine mode, and all particles larger than 0.6 μm as coarse mode; that cutoff is not a good choice for all size distributions. It appears from the AERONET size distribution plot for 8 February 2004 (Figure 8) that all retrieved particles larger than 0.2 μm radius fell into the coarse mode bin, including a possible third mode that peaks around 0.75 μm radius.

[41] AERONET-retrieved spherical and spheroidal size distributions, available for the 6 and 8 February 2004 events are almost identical (see Figure 8), except for a particle component having $r_v < 0.2$ μm in the spherical but not the spheroidal retrievals [*Dubovik et al.*, 2002a, 2002b]. The MISR result is supported by our expectation that nonspherical particles dominate the atmospheric column on these dates, and that the AERONET retrievals that include nonspherical particles give results more in agreement with MISR, though AERONET values are still skewed lower. This may amount to differences in the mineral dust models used in the two retrievals. We hope to address this issue further once we have coincident AERONET, MISR, and field data.

[42] MISR–retrieved optical depths and Angstrom exponents are in good agreement with AERONET measured values, as shown in Figure 9 and Table 5. Note that MISR retrieves a small value of the Angstrom exponent even when

Figure 6. Size-mode ratio sensitivity plots for medium-mode grains, part 2. Here the comparison space contains a range of large-mode SSA options along with the medium-mode particles. The plots are arranged in four pairs of bar charts, similarly to Figure 5. The simulated atmosphere for each group contains a medium-mode (r_0 = 0.5 μm) grain-shaped component and a large-mode (M2, r_0 = 1 μm) spheroid-shaped component, mixed in midvisible AOT proportions of (a) 20%–80%, (b) 40%–60%, (c) 60%–40%, and (d) 80%–20%, all components having 2% internally mixed hematite. The comparison space includes these components plus a large-mode (M2, r_0 = 1 μm) spheroid-shaped components having 4% and 10% internally mixed hematite; all other components in this set of tests contain 2% internally mixed hematite.

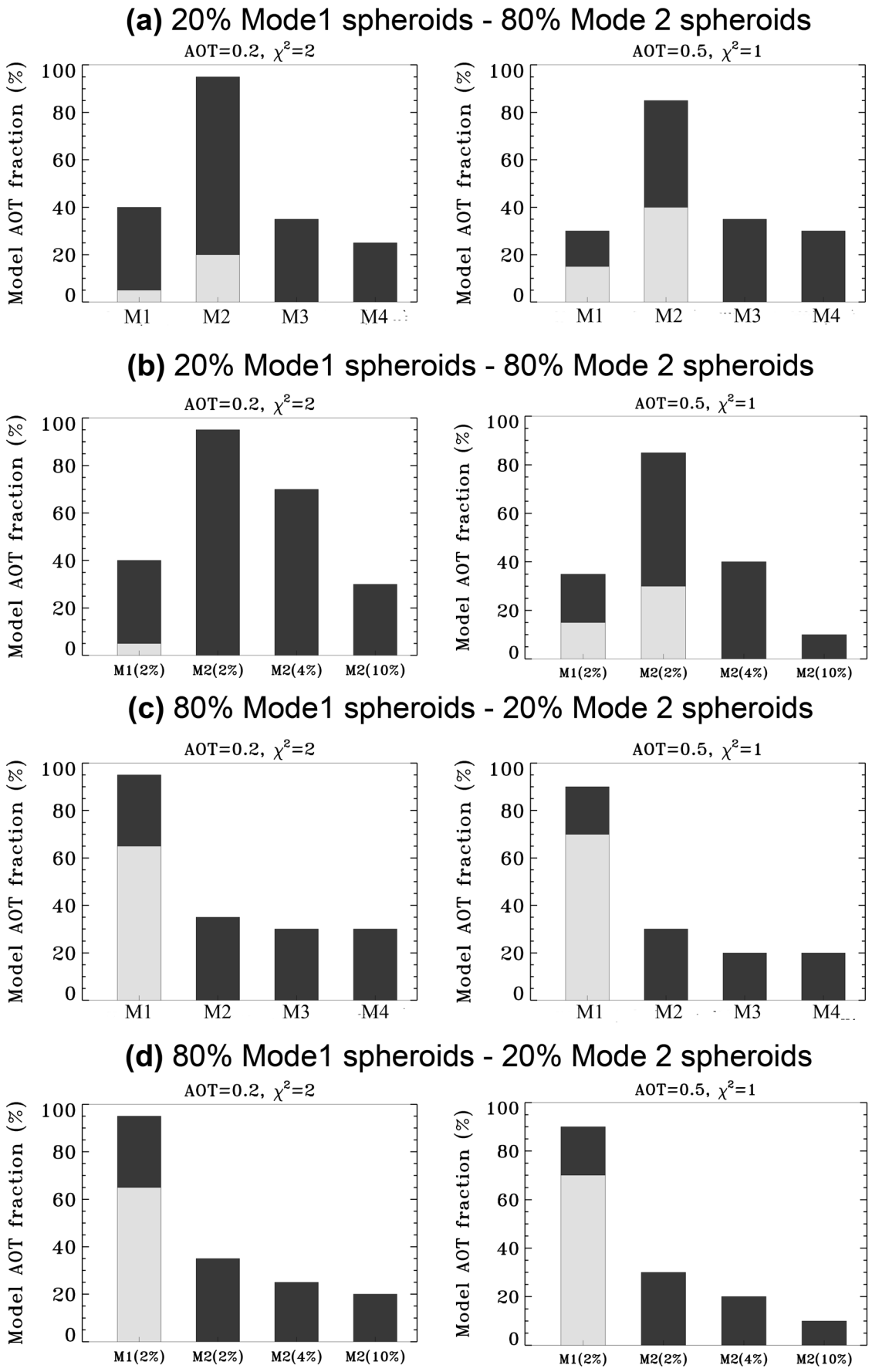
(a) 20% Mode1 spheroids - 80% Mode 2 spheroids
AOT=0.2, χ^2=2
AOT=0.5, χ^2=1
Model AOT fraction (%)
0
20
40
60
80
100
M1
M2
M3
M4
(b) 20% Mode1 spheroids - 80% Mode 2 spheroids
AOT=0.2, χ^2=2
AOT=0.5, χ^2=1
Model AOT fraction (%)
M1(2%)
M2(2%)
M2(4%)
M2(10%)
(c) 80% Mode1 spheroids - 20% Mode 2 spheroids
AOT=0.2, χ^2=2
AOT=0.5, χ^2=1
Model AOT fraction (%)
M1
M2
M3
M4
(d) 80% Mode1 spheroids - 20% Mode 2 spheroids
AOT=0.2, χ^2=2
AOT=0.5, χ^2=1
Model AOT fraction (%)
M1(2%)
M2(2%)
M2(4%)
M2(10%)

Figure 7

Table 2. MISR Overpass and AERONET Cape Verde Site Data Sampling Locations and Timing for Five Dust Events Where Coincident Observations Were Taken

Day	AERONET Retrieval Notes	MISR Orbit Path	MISR Overpass Time, UTC	AERONET Sky-Scan Collection Time	Location		
					AERONET, deg	MISR Patch 1, deg	MISR Patch 2, deg
26 May 2003	AOT ~ 0.3; r_V ~ 1.4 μm, σ ~ 1.1	18278, path 210	1131	1130:19	16.733N, 22.935W	16.39N, 22.45W	16.42N, 22.64W
11 Jun 2003	AOT ~ 0.3; r_V ~ 1.4 μm, σ ~ 1.1	18511, path 210	1131	1132:43	16.733N, 22.935W	16.71N, 22.58W	16.52N, 22.04W
6 Feb 2004	AOT ~ 0.5; r_V ~ 1.2 μm, σ ~ 1.0	22006, path 210	1132	1148:37	16.733N, 22.935W	17.11N, 22.32W	17.58N, 22.49W
8 Feb 2004	AOT ~ 0.5; bimodal size distribution	22035, path208	1119	1148:47	16.733N, 22.935W	16.46N, 22.44W	16.34N, 22.52W
6 Jun 2003	AOT > 1.0; r_V ~ 1 μm, σ ~ 1.0	23768, path 209	1125	1132:05	16.733N, 22.935W	16.33N, 22.61W	16.41N, 22.49W

MISR retrieves primary medium particles, as does AERONET, reflecting the almost flat wavelength dependence of dust model extinction coefficients as shown in Table 1. On 6 June, when the AERONET-reported optical depth is high, MISR retrieves an AOT approximately 0.1 higher than AERONET, and there is about a 0.05 difference between the MISR AOTs for the two selected patches. This is probably due to actual AOT spatial variability, which is expected for such heavy dust events, and can be seen in highly stretched versions of the MISR images. Similarly, MISR AOT values on 8 February are lower by ~0.05, which may be explained by the difference between the MISR and AERONET data collection times for this event, or the absence of a very fine size mode in the MISR retrieval's assumed climatolgy.

[43] Table 5 indicates that MISR-retrieved SSA is in reasonable agreement with the available AERONET retrieval results that include spheroidal particles (6 and 8 February 2004). However, the MISR values are not in good agreement with AERONET-reported values derived with spherical-only particle models. In the spherical-only AERONET cases, the MISR-retrieved quantities are larger than those obtained by AERONET, as expected. Figure 10 contrasts the MISR retrievals along with both the AERONET spherical-only and spheroidal results for 6 and 8 February 2004.

[44] To test the performance of the new [*Kalashnikova et al.*, 2005] dust models in the MISR Standard Retrieval, we compared the MISR standard AOT product (version 15) that used the old dust models, with the more recent version 16 product that includes the new models, for all five events studied here. We find the MISR AOT retrieval coverage significantly improves over dusty regions, as illustrated by Figure 11 for the 6 February 2004 event. For all five events, the MISR standard retrieval selected the new dust models as the best fitting for dust plumes, and spherical models for nondusty areas. This is also a further demonstration of MISR's ability to distinguish spherical from nonspherical particles over ocean surfaces.

[45] With the MISR Research Aerosol retrieval, we have shown that over dark water, the MISR data contains information about particle shape, and can distinguish grain-like dust components from spherical, plate-like, and spheroidal components. Retrieved MISR AOT and Angstrom exponent are in reasonable agreement with those measured by AERONET. Some apparent MISR biases in the retrieved AOT are likely explained by dust AOT variability [e.g., *Christopher and Wang*, 2004]. As predicted by our theoretical sensitivity studies, in actual dust events over dark water, MISR can reliably distinguish grains from plates, spheroids, and spheres, even of the same composition, and can separate three to five size classes within the $PM_{2.5}$ range. As expected, MISR is not able to separate medium-sized particles having 1, 2 and 4% hematite, but can distinguish these from 10% hematite, which translates into a sensitivity of about 0.05 in SSA. Also as expected, the retrievals obtained large-mode dust AOT fractions lower than 20% far from the dust sources. In all cases, mixtures that passed the $\chi^2_{max} < 2$ criterion included the new medium-sized grain-like nonspherical dust models having 1, 2, or 4% hematite.

4. Conclusions

[46] We tested MISR theoretical sensitivity to AOT, particle shape, SSA, and ratio of medium to large dust particle optical models. The study demonstrates that over

Figure 7. Size-mode ratio sensitivity plots for medium-mode ellipsoids, with a range of large-mode size options along with the medium-mode particles in the comparison space. The plots are arranged in four pairs of bar charts, similarly to Figure 3. The simulated atmosphere for each pair contains a medium-mode (r_0 = 0.5 μm) spheroid-shaped component and a large-mode (M2, r_0 = 1 μm) spheroid-shaped component, mixed in midvisible AOT proportions of (a, b) 20%–80% and (c, d) 80%–20%, all components having 2% internally mixed hematite. The comparison space includes these components plus, for Figures 7a and 7c, M3 (r_0 = 1.5 μm) and M4 (r_0 = 2 μm) large-mode, spheroid-shaped components containing 2% internally mixed hematite and, for Figures 7b and 7d, large-mode (M2, r_0 = 1 μm) spheroid-shaped components having 4% and 10% internally mixed hematite.

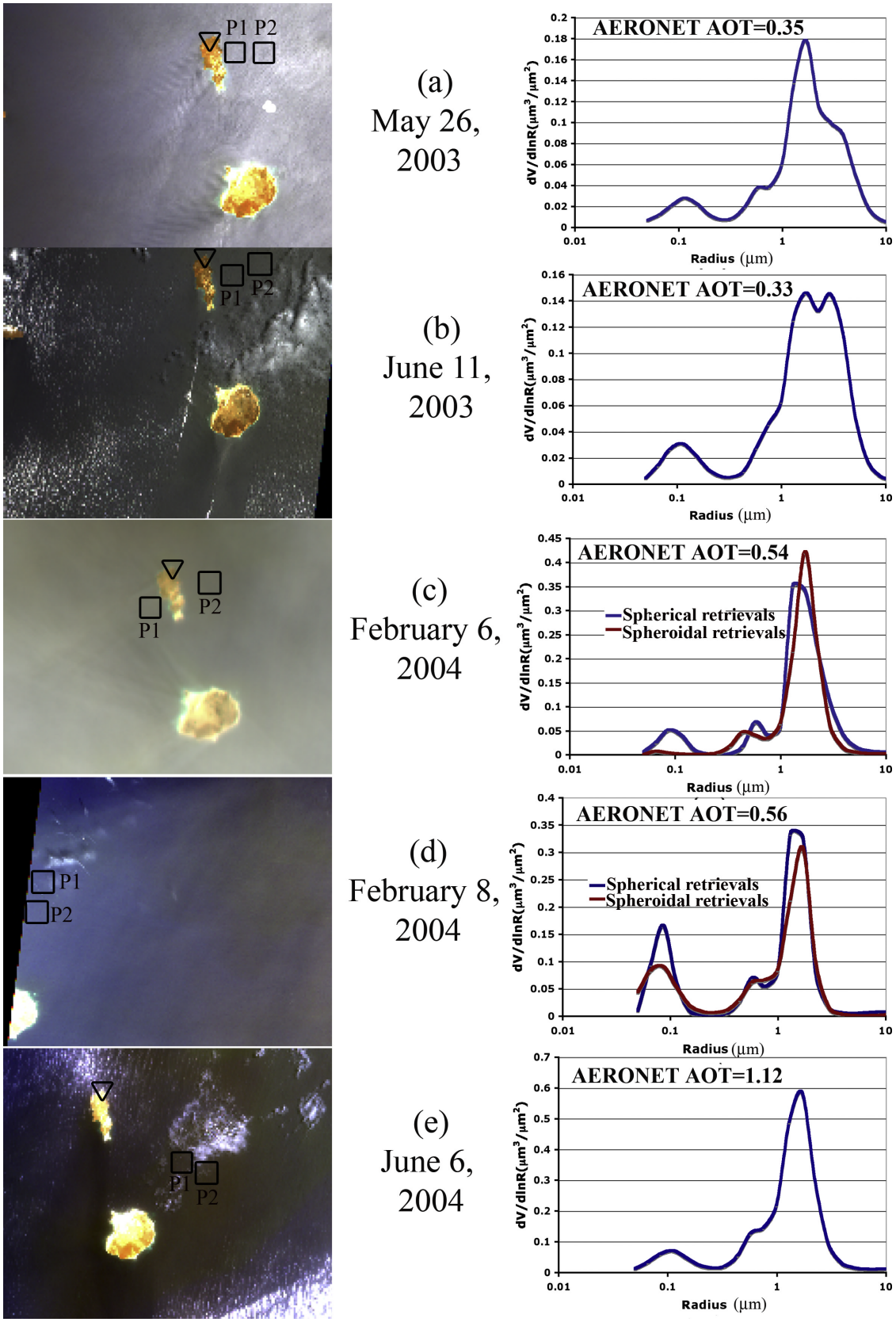

Figure 8. Five dust events observed by MISR around the Cape Verde AERONET site. The 3 by 3 pixel MISR analysis patches are shown, along with the AERONET-derived volume-weighted aerosol size distributions for each event. The midvisible AOT at the AERONET site is indicated within each size distribution plot.

Table 3. Aerosol Models, in Addition to the Dust Models From Table 1, Included in the Research Aerosol Retrieval Algorithm Climatology for the Cape Verde Island Event Analysis

Name	Shape	r_0, μm	r_V, μm	r_{eff}, μm	σ	σ_{ext}, 0.672 μm	σ_{ext}, 0.866 μm	w_0, 0.672 μm	w_0, 0.866 μm
Thin_cirrus (hexagonal_columns)	polyhedral	. . ..	40.03	21.56	. . .	2.535	2.535	1.00	1.00
Sulfates1	sphere	0.06	0.16	0.12	1.70	0.445	0.235	1.00	1.00
Sulfates2	sphere	0.12	0.36	0.26	1.75	1.768	1.242	1.00	1.00
Sea salt	sphere	0.5	1.85	1.28	1.85	2.602	2.743	1.00	1.00

ocean, for near-surface wind speeds up to 5 m/s and total column midvisible AOT about 0.15 or higher, MISR can distinguish among medium-sized plate, grain, and spheroid dust model components, provided the component contributes at least 15–20% to the total AOT, and it can separate spheres from plates, grains, and spheroids, with an uncertainty of less than 10%. Under natural conditions over dark water, MISR cannot distinguish dust particles having 1, 2, or 4% hematite because these dust compositional types all absorb weakly in the red and near-infrared channels (red channel SSA in the range of 0.98–0.99). However MISR can distinguish between strongly absorbing dust having 10% hematite (red channel SSA of about 0.94) and the weakly absorbing dust models with uncertainty less than 10% for dust midvisible optical depths higher than 0.5, and with an uncertainty less than 20% for optical depths greater than about 0.15. Sensitivity tests for bimodal dust distributions show that MISR can distinguish between medium and large dust modes, and is sensitive to the properties of each mode that contributes at least 20% to the total column midvisible AOT.

[47] Near-coincident MISR and AERONET observations of Saharan dust plumes over dark water confirm our theoretical findings regarding MISR sensitivity to particle properties, and show that low-absorbing grain-like particles provide the best fit to the MISR-measured radiances for these events. MISR AOTs for these cases agree with AERONET-measured values within a 0.02 range; differences of ~0.06, which were observed for a heavy dust event (AOT > 0.1), and for a case when the AERONET retrieval

Table 4. Best Fitting Aerosol Mixtures From the MISR Research Retrieval for the Five Cape Verde Dust Events, Summarized Together With MISR- and AERONET-Retrieved Size Parameters[a]

Day	Retrieval Location	Selected Models	AOT Fraction	χ^2_{abs}	$r_{eff\ MISR}$, μm	Nearby $r_{eff\ AERONET}$, μm	$r_{V\ MISR}$, μm	Nearby $r_{V\ AERONET}$, μm
26 May 2003	patch 1	grain_1p_M1	70%	1.13	0.79	0.60	0.95	1.36
		sphroidal_1p_M2	10%					
		sulfates1	20%					
	patch 2	grain_4p_M1	60%	1.05	0.73	0.60	0.94	1.36
		sea salt	20%					
		sulfates1	20%					
11 Jun 2003	patch 1	grain_1p_M1	25%	1.13	1.18	0.60	1.50	1.45
		sphroidal_1p_M2	30%					
		sulfates1	15%					
		sea salt	20%					
	patch 2	grain_4p_M1	55%	1.07	0.59	0.60	0.81	1.45
		sea salt	30%					
		sulfates1	15%					
6 Feb 2004	patch 1	grain_2p_M1	95%	1.87	0.72	0.57 (0.88)	0.85	1.24
		sulfates1	5%					(1.41)
	patch 2	grain_1p_M1	100%	2.00	0.75	0.57 (0.88)	0.89	1.24
								(1.41)
8 Feb 2004	patch 1	grain_1p_M1	70%	1.24	0.69	0.27 (0.26)	0.92	0.68
		sea salt	15%					(0.67)
		sulfates1	15%					
	patch 2	grain_1p_M1	70%	0.85	0.76	0.27 (0.26)	0.98	0.68
		sphroidal_1p_M2	5%					(0.67)
		sulfates1	15%					
		sea salt	10%					
6 Jun 2004	patch 1	grain_1p_M1	75%	0.37	0.79	0.55	1.01	1.1
		sphroidal_1p_M2	5%					
		sulfates1	10%					
		sea salt	10%					
	patch 2	grain_4p_M1	80%	1.05	0.71	0.55	0.91	1.1
		sea salt	10%					
		sulfates1	10%					

[a]Abbreviations are as follows: $r_{eff\ MISR}$, $r_{eff\ AERONET}$, MISR- and AERONET-retrieved effective radius values, respectively; $r_{V\ MISR}$, $r_{V\ AERONET}$, MISR and AERONET volume-weighted radius values, respectively. AERONET available spheroidal retrievals are shown in parentheses.

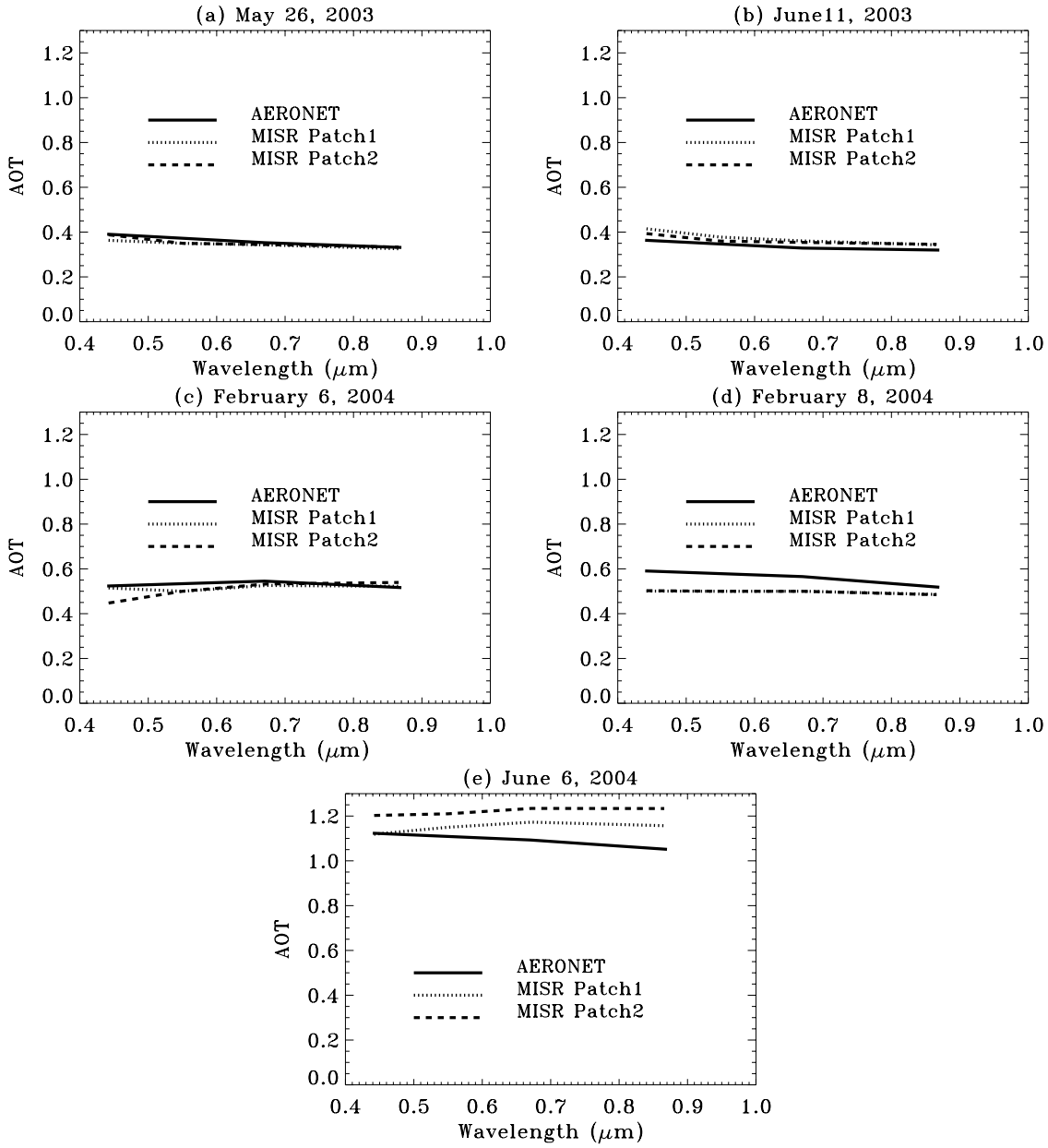

Figure 9. Comparisons between AERONET-retrieved spectral AOT values and those derived with the MISR Research Retrieval over the nearby patches marked in Figure 8, for five Cape Verde dust events.

indicated a significant proportion of very small aerosols, are likely due to dust spatial variability during heavy dust outbreaks and MISR's limited sensitivity to particles <0.1 μm radius, respectively. MISR Angstrom exponents are very small (±0.2), as expected for dust events, and in agreement with near-simultaneous AERONET measurements. MISR-retrieved size distributions are in general agreement with those obtained by AERONET when medium-sized particles are observed. However, MISR is less sensitive to particles with radii less than about 0.1 μm and larger than about 1 μm. AERONET SSA retrievals that allow only spherical particles when nonspherical dust is a dominant component seem to underestimate particle SSA, whereas when spheroidal components are included, the SSA results are in good agreement (±0.02) with the MISR values. The range of ±0.02 in retrieved SSA values is an expected upper limit for MISR-like satellite observations. The case studies suggest that a good medium-mode dust optical model for the MISR operational retrieval is a medium-sized grain particle having 1% or 2% hematite.

[48] Determining particle microphysical properties from space-based, passive remote sensing is at the cutting edge of aerosol research. In this paper, we have demonstrated the ability to retrieve AOT and SSA during significant dust events (AOT > 0.15) within 10 to 20% of near-coincident AERONET values. We used the new dust aerosol optical models and the MISR Research Aerosol Retrieval

Table 5. Summary of MISR and AERONET Red and NIR Band Aerosol Optical Thicknesses, Angstrom Exponents, and Single-Scattering Albedos for the Five Cape Verde Dust Events[a]

		MISR AOT		AERONET AOT				MISR SSA		AERONET SSA	
Day	Retrieval Locations	Red	NIR	Red	NIR	MISR α	AERONET α	Red	NIR	Red	NIR
26 May 2003	patch 1	0.342	0.325	0.352	0.331	0.161	0.238	0.993	0.996	0.889	0.884
	patch 2	0.344	0.333	0.352	0.331	0.216	0.238	0.987	0.994	0.889	0.884
11 Jun 2003	patch 1	0.360	0.343	0.329	0.319	0.248	0.193	0.940	0.944	0.892	0.891
	patch 2	0.354	0.345	0.329	0.319	0.185	0.193	0.936	0.942	0.892	0.891
6 Feb 2004	patch 1	0.526	0.522	0.545	0.516	−0.04	0.09	0.991	0.995	0.969 (0.980)	0.973 (0.984)
	patch 2	0.532	0.539	0.545	0.516	−0.28	0.09	0.994	0.997	0.969 (0.980)	0.973 (0.984)
8 Feb 2004	patch 1	0.500	0.485	0.565	0.518	0.04	0.18	0.996	0.998	0.934 (0.978)	0.940 (0.981)
	patch 2	0.499	0.484	0.565	0.518	0.05	0.18	0.995	0.997	0.934 (0.978)	0.940 (0.981)
6 Jun 2004	patch 1	1.172	1.115	1.093	1.052	0.05	0.09	0.994	0.997	0.897	0.898
	patch 2	1.234	1.233	1.093	1.052	0.03	0.09	0.984	0.991	0.897	0.898

[a]Abbreviations are as follows: NIR, near-infrared; AOT, aerosol optical thickness; SSA, single-scattering albedo; α, Angstrom exponent. AERONET available spheroidal retrievals are shown in parentheses.

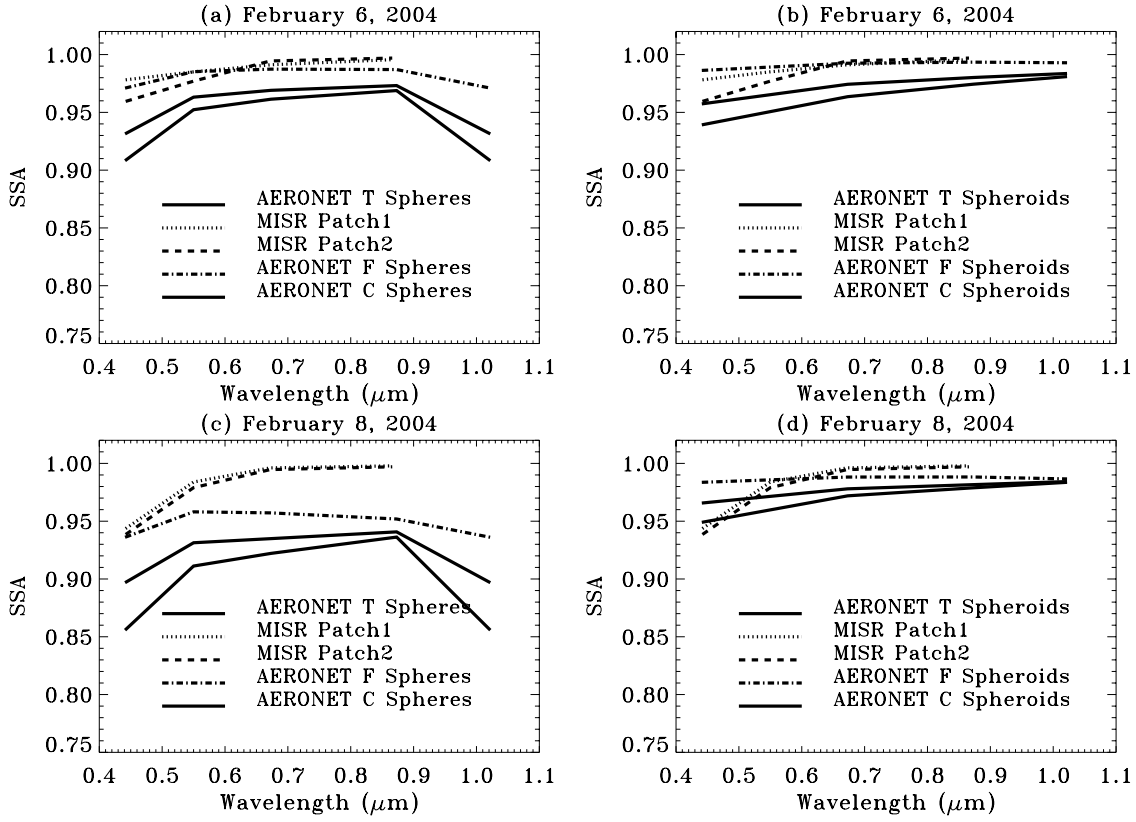

Figure 10. Comparisons between AERONET-retrieved spectral SSA and values derived with the MISR Research Retrieval for the (a, b) 6 February and (c, d) 8 February 8 2004 events. Figures 10a and 10c show AERONET retrievals done with spherical models, and Figures 10b and 10d show AERONET retrievals done with spheroidal models. AERONET-T, total SSA; AERONET-F, SSA for the fine aerosol fraction; AERONET-C, SSA for the coarse aerosol fraction.

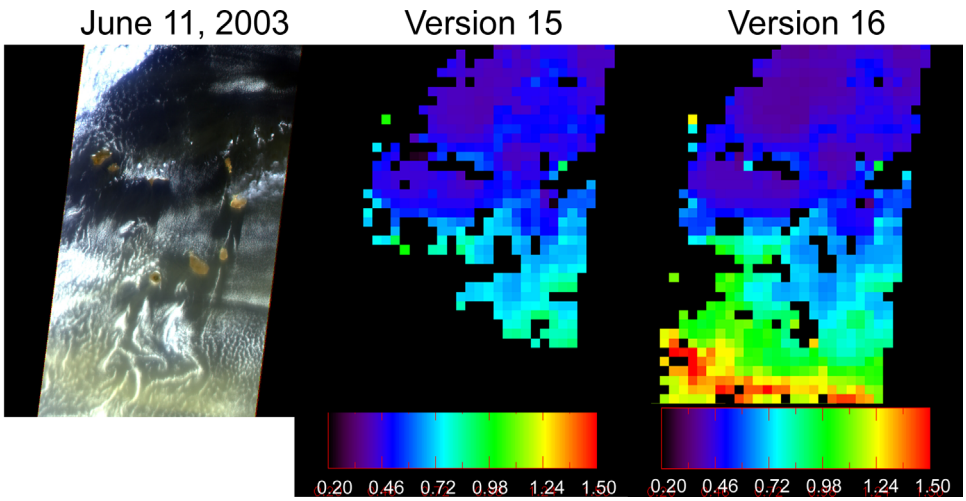

Figure 11. Comparison of MISR Standard Aerosol midvisible AOT product derived (left) with the old dust models (version 15) and (right) with the new dust models (version 16) for the Cape Verde event on 11 June 2003.

algorithm, which allows us to individually select 3.3 by 3.3 km pixel patches, to independently determine them to be cloud-free and homogeneous, and to make more flexible choices about particle components and mixtures than the MISR Standard algorithm. MISR SSA and particle size accuracy, though not necessarily AOT accuracy, might be lower for the MISR Standard 17.6 km aerosol products. MISR Standard aerosol property product refinement and validation are currently underway.

[49] **Acknowledgments.** We thank Wen-Hao Li for his help in creating MISR Research Aerosol Retrieval results for an early version of this study and the MISR team for providing facilities, access to data, and useful discussions. The work of O.V.K. is supported in part by a National Research Council postdoctoral fellowship at the Jet Propulsion Laboratory and in part by a grant from the NASA Earth Sciences Division, Climate and Radiation program, under H. Maring. R.K. is supported in part by the NASA Earth Sciences Division, Climate and Radiation program, under H. Maring, and in part by the NASA Earth Observing System Multiangle Imaging SptectroRadiometer project, D. Diner, Principal Investigator. We thank the AERONET project and the AERONET Cape Verde station Principal Investigator, Didier Tanré, for their efforts in establishing and maintaining this site and for sharing these valuable data. This work was performed at the Jet Propulsion Laboratory, California Institute of Technology, under contract with NASA. The MISR data were obtained from the NASA Langley Research Center Atmospheric Sciences Data Center.

References

Bruegge, C. J., W. A. Abdou, D. J. Diner, B. J. Gaitley, M. C. Helmlinger, R. A. Kahn, and J. V. Martonchik (2004), Validating the MISR radiometric scale for the ocean aerosol science communities, in *Post-launch Calibration of Satellite Sensors*, edited by S. A. Morain and A. M. Budge, pp. 103–115, A. A. Balkema, Brookfield, Vt.

Christopher, S., and J. Wang (2004), Inter-comparison between MISR and Sanphotometer AOT in dust source regions over China: Implications to satellite retrievals and radiative forcing calculations, *Tellus, Ser. B*, *56*, 451–456.

Clarke, A. D., et al. (2004), Size distributions and mixtures of dust and black carbon aerosol in Asian outflow: Physiochemistry and optical properties, *J. Geophys. Res.*, *109*, D15S09, doi:10.1029/2003JD004378.

Diner, D. J., et al. (1998), Multi-angle Imaging SpectroRadiometer (MISR) instrument description and experiment overview, *IEEE Trans. Geosci. Remote Sens.*, *36*, 1072–1087.

Diner, D. J., et al. (2005), The value of multi-angle measurements for retrieving structurally and radiatively consistent properties of clouds, aerosols, and surfaces, *Remote Sens. Environ.*, *97*, 495–518.

Draine, B. T., and J. P. Flatau (1994), Discrete-dipole approximation for scattering calculations, *J. Opt. Soc. Am. A*, *11*, 1491–1499.

Dubovik, O., and M. D. King (2000), A flexible inversion algorithm for retrieval of aerosol optical properties from Sun and sky radiance measurements, *J. Geophys. Res.*, *105*, 20,673–20,696.

Dubovik, O., B. Holben, T. F. Eck, A. Smirnov, Y. J. Kaurman, M. E. King, D. Tanre, and I. Slutsker (2002a), Variability of absorption and optical properties of key aerosol types observed in worldwide locations, *J. Atmos. Sci.*, *59*, 590–608.

Dubovik, O., B. N. Holben, T. Lapyonok, A. Sinyuk, M. I. Mishchenko, P. Yang, and I. Slutsker (2002b), Non-spherical aerosol retrieval method employing light scattering by spheroids, *Geophys. Res. Lett.*, *29*(10), 1415, doi:10.1029/2001GL014506.

Holben, B. N., et al. (1998), AERONET—A federated instrument network and data archive for aerosol characterization, *Remote Sens. Environ.*, *66*, 1–16.

Intergovernmental Panel on Climate Change (2001), IPCC summary for policymakers: A report of working group of the Intergovernmental Panel on Climate Change, technical report, World Meteorol. Organ., Geneva.

Kahn, R., R. West, D. McDonald, B. Rheingans, and M. I. Mishchenko (1997), Sensitivity of multiangle remote sensing observations to aerosol sphericity, *J. Geophys. Res.*, *102*, 16,861–16,870.

Kahn, R., P. Banerjee, D. McDonald, and D. J. Diner (1998), Sensitivity of multiangle imaging to aerosol optical depth and to pure-particle size distribution and composition over ocean, *J. Geophys. Res.*, *103*(D24), 32,195–32,238.

Kahn, R., P. Banerjee, and D. McDonald (2001a), Sensitivity of multiangle imaging to natural mixtures of aerosols over ocean, *J. Geophys. Res.*, *106*, 18,219–18,238.

Kahn, R., P. Banerjee, D. McDonald, and J. Martonchik (2001b), Aerosol properties derived from aircraft multiangle imaging over Monterey Bay, *J. Geophys. Res.*, *106*, 11,977–11,995.

Kahn, R., et al. (2004), Environmental snapshots from ACE-Asia, *J. Geophys. Res.*, *109*, D19S14, doi:10.1029/2003JD004339.

Kahnert, M., T. Nousiainen, and B. Veihelmann (2005), Spherical and spheroidal model particles as an error source in aerosol climate forcing and radiance computations: A case study for feldspar aerosols, *J. Geophys. Res.*, *110*, D18S13, doi:10.1029/2004JD005558.

Kalashnikova, O. V., R. Kahn, I. N. Sokolik, and W.-H. Li (2005), Ability of multiangle remote sensing observations to identify and distinguish mineral dust types: Optical models and retrievals of optically thick plumes, *J. Geophys. Res.*, *110*, D18S14, doi:10.1029/2004JD004550.

Martonchik, J. V., D. J. Diner, R. Kahn, T. P. Ackerman, M. M. Verstraete, B. Pinty, and H. R. Gordon (1998), Techniques for the retrieval of aerosol properties over land and ocean using multi-angle imaging, *IEEE Trans. Geosci. Remote Sens.*, *36*, 1212–1227.

Martonchik, J. V., D. J. Diner, K. A. Crean, and M. A. Bull (2002), Regional aerosol retrieval results from MISR, *IEEE Trans. Geosci. Remote Sens.*, *40*, 1520–1531.

Mishchenko, M. I., A. A. Lacis, B. E. Carlson, and L. D. Travis (1995), Nonsphericity of dust-like tropospheric aerosols: Implication for aerosol remote sensing and climate modeling, *Geophys. Res. Lett.*, *22*, 1077–1080.

Mishchenko, M. I., L. D. Travis, R. A. Kahn, and R. A. West (1997), Modeling phase functions for dustlike tropospheric aerosols using a shape mixture of randomly oriented polydisperse spheroids, *J. Geophys. Res.*, *102*, 16,831–16,847.

Mishchenko, M. I., L. D. Travis and A. A. Lacis (2002), *Scattering, Absorption and Emission of Light by Small Particles*, Cambridge Univ. Press, New York.

Sokolik, I. N., and O. B. Toon (1999), Incorporation of mineralogical composition into models of the radiative properties of mineral aerosol from UV to IR wavelengths, *J. Geophys. Res.*, *104*, 9423–9444.

Takano, Y., and K.-N. Liou (1989), Solar radiative transfer in cirrus clouds: part I. Single-scattering and optical properties of hexagonal ice crystals, *J. Atmos. Sci.*, *46*, 3–19.

Volten, H., O. Muñoz, E. Rol, J. F. de Haan, W. Vassen, J. W. Hovenier, K. Muinonen, and T. Nousiainen (2001), Scattering matrices of mineral aerosol particles at 441.6 nm and 632.8 nm, *J. Geophys. Res.*, *106*, 17,375–17,402.

R. Kahn and O. V. Kalashnikova, Jet Propulsion Laboratory, California Institute of Technology, 4800 Oak Grove Drive, Pasadena, CA 91109, USA. (olga.v.kalashnikova@jpl.nasa.gov)